

Multi-component strongly attractive Fermi gas: a color superconductor in a one-dimensional harmonic trap

Xia-Ji Liu^{1,2}, Hui Hu², and Peter D. Drummond¹

¹ *ARC Centre of Excellence for Quantum-Atom Optics, School of Physical Sciences,
University of Queensland, Brisbane, Queensland 4072, Australia*

² *Department of Physics, Renmin University of China, Beijing 100872, China*
(Dated: June 21, 2024)

Recent advances in ultra-cold atomic Fermi gases make it possible to achieve a fermionic superfluid with multiple spin components. In this context, any mean-field description is expected to fail, owing to the presence of tightly bound clusters or molecules that consist of more than two particles. Here we present a detailed study of a strongly interacting multi-component Fermi gas in a highly elongated or quasi-one-dimensional harmonic trap, which could be readily obtained in experiment. By using the exact Bethe ansatz solution and a local density approximation treatment of the harmonic trap, we investigate the equation of state of the multi-component Fermi gas in both a homogeneous and trapped environment, as well as the density profiles and low-energy collective modes. The binding energy of multi-component bound clusters is also given. We show that there is a peak in the collective mode frequency at the critical density for a deconfining transition to a many-body state that is analogous to the quark color superconductor state expected in neutron stars.

PACS numbers: 03.75.Ss, 05.30.Fk, 71.10.Pm, 74.20.Fg

I. INTRODUCTION

Recent experimental progress achieved in trapped ultra-cold atomic gases provides a great opportunity for exploring strongly interacting many-body physics. Owing to the molecular Feshbach resonance [1], the strength of the interactions between atoms in different hyperfine states (or species) can be arbitrarily changed from strong to weak coupling in a well-controlled manner. Moreover, interactions can be effectively tuned by using optical lattices with a varying tunneling barrier [2]. Consequently, a number of many-body models in condensed matter physics and nuclear physics can be readily accessed in the ultra-cold atomic gases. In the past few years, considerable interest has been focused on trapped two-component Fermi gases close to a broad Feshbach resonance. In particular, the crossover from Bardeen-Cooper-Schrieffer (BCS) fermionic superfluidity of Cooper pairs to Bose-Einstein condensation (BEC) of tightly bounded molecules has been explored in great detail [3, 4, 5, 6, 7, 8, 9, 10, 11, 12, 13, 14, 15, 16, 17, 18].

Multi-component Fermi gases with more than two species can be easily trapped and manipulated as well. For this type of Fermi gas, bound *multi-body* clusters are expected to appear above a critical interaction strength [19], in addition to the formation of Cooper pairs due to two-body “pairing correlations”. As is well known, a landmark theoretical result in quantum physics is Efimov’s prediction of a universal set of bound trimer states appearing for three identical bosons with a resonant two-body interaction [20]. The existence of such an Efimov resonance greatly changes the properties of dilute Bose gases, as observed recently in an ultracold gas of cesium atoms [21]. Similarly, multi-body clusters are of fundamental importance to fermionic superfluidity in multi-component Fermi gases. While Cooper pairs are dom-

inant in the weak coupling limit, an exotic superfluid state with bound multi-body clusters should emerge in the strong coupling regime. In between, a quantum phase transition is then anticipated to take place [22], in contrast to the smooth crossover observed in the two-component case [3].

This issue is relevant to outstanding problems in nuclear and particle physics. The quark model of nuclear matter at low density describes nucleons as three fermion clusters: tri-quark bound states. At sufficiently high density and pressure, it is conjectured that a phase-transition occurs to a deconfined color superfluid phase of quark matter [23, 24]. This is believed to occur in the interior of neutron stars and possibly in heavy-ion collisions. While quark matter has many other features, it is interesting to find that a physically accessible system of interacting ultra-cold fermions is also expected to display these features of multi-body fermion clusters and quantum phase-transitions. Ultra-cold atoms could provide a means to test these theoretical predictions. If confirmed, this would lend support to current ideas in particle theory and astrophysics.

However, the role of multi-body bound states is generally not well understood theoretically. Their description is beyond the generally adopted mean-field framework, which handles competition between two-body correlations among different atom pairs. This, however, is of importance only in the weak coupling limit. For strong coupling, the use of numerical Monte Carlo techniques is hampered by the fermionic sign problem [25]. It is therefore of great importance to have an analytically soluble model of multi-component Fermi gases, and to study both the weakly and strongly interacting regimes on an equal footing. An exact analysis is provided in this paper for the case of multi-component Fermi gases in one dimension (1D), where multi-body bound clusters are al-

ways present, regardless of the interaction strength.

As well as being exactly soluble, the 1D problem has great experimental relevance. A quantum degenerate trapped two-component Fermi gas in quasi 1D has been demonstrated recently by loading an ultra-cold Fermi gas into a two-dimensional optical lattice [26] of trapping ‘tubes’. In this configuration, the radial motion of atoms perpendicular to each tube is frozen to zero-point oscillations due to tight transverse confinement, while axial motion is only weakly confined. One then obtains an array of effective 1D systems, each in an axial harmonic trap. The manipulation of more than two species in 1D is within reach of present-day technology, and is likely to be achieved soon in experiments.

A typical example of these developments is lithium gas [27], which has favorable collisional properties among its lowest three hyperfine spin states, denoted $|1\rangle$, $|2\rangle$ and $|3\rangle$, respectively. A recent accurate measurement of the scattering lengths between these hyperfine states shows that the background interactions are anomalously large [27], with background scattering lengths about $-1500a_0$, where a_0 ($= 0.0529177$ nm) is the Bohr radius. There are also three broad s -wave Feshbach resonances located at the positions $B = 834, 811$, and 690 Gauss for $(1, 2)$, $(2, 3)$, and $(3, 1)$ channels, respectively. These peculiar collisional properties are useful to cool the gas down to the quantum degenerate regime. Ideally, one expects experimentally accessible lowest temperatures for this three-state mixture to be in the same range as for two-component ensembles, *i.e.*, $T \simeq 0.05T_F$, where T_F is the Fermi temperature of an ideal Fermi gas. Thus, a novel fermionic multi-component superfluid may be anticipated. For this reason, three-component lithium gas has attracted a great deal of theoretical interest, including analysis of mean-field states [28, 29, 30, 31, 32] as well as phase diagrams [22, 33, 34, 35, 36].

Here, we report on properties of a multi-component Fermi gas in 1D. Firstly, using the exact Bethe ansatz solution [37, 38, 39, 40], we investigate the exact ground state of a homogeneous gas with attractive interactions at zero temperature. To make contact with experiments, we then consider an inhomogeneous Fermi gas under harmonic confinement, within the framework of the local density approximation (LDA). The equation of state of the system in both the uniform and trapped case are investigated in detail. Particular attention is drawn to the density profiles and low-lying collective modes of the trapped cloud, which are readily measurable in experiment. We show that the gas becomes more attractive as the number of species increases, demonstrating the strongly interacting nature of multi-body bound clusters.

The paper is organized as follows. In the following section, we outline the theoretical model for a 1D multi-component Fermi gas. Of particular relevance for an experimental realization is our calculation of the effective 1D coupling constant for the three-component lithium gases. In Sec. III, we present the exact Bethe ansatz solution and discuss the equation of state and the sound

velocity of a uniform system at zero temperature. In Sec. IV, using the LDA method we investigate the density profile and the equation of state in the trapped environment. Also, we describe the dynamics of trapped gases in terms of 1D hydrodynamic equations and develop a novel algorithm to solve these equations. The behavior of low-lying collective modes is then obtained and discussed. We end with some concluding remarks in Sec. V. An appendix is used to outline the details of the algorithm used in solving the 1D hydrodynamic equations.

II. MODELS

A quasi-1D multi-component Fermi gas in a highly elongated trap can be formed using a two-dimensional optical lattice [26]. By suitably tuning the lattice depth, the anisotropy aspect ratio $\lambda = \omega_z/\omega_\rho$ of two harmonic frequencies can become extremely small. This means that the Fermi energy associated with the longitudinal motion of the atoms is much smaller than the energy level separation along the transverse direction, *i.e.*, $N\hbar\omega_z \ll \hbar\omega_\rho$ and $k_B T \ll \hbar\omega_\rho$, where N is the total number of atoms. In this limit, the transverse motion will be essentially frozen out, and one ends up with a quasi-one dimensional system.

A. Interaction Hamiltonian

We study a gas with pseudo-spin $S = (\kappa - 1)/2$, where κ (≥ 2) is the number of components. From now we shall assume that the fermions in different spin states attract each other via the *same* short-range potential $g_{1D}\delta(x)$. Denoting the mass of each fermion as m , with a total fermion number $N = \sum_{l=1}^{\kappa} N_l$ (where N_l is the number of fermions with pseudo-spin projection l) the first quantized Hamiltonian for the system is therefore

$$\mathcal{H} = \mathcal{H}_0 + \sum_{i=1}^N \frac{1}{2} m \omega^2 x_i^2. \quad (2.1)$$

Here

$$\mathcal{H}_0 = -\frac{\hbar^2}{2m} \sum_{i=1}^N \frac{\partial^2}{\partial x_i^2} + g_{1D} \sum_{i < j} \delta(x_i - x_j) \quad (2.2)$$

represents the part of Hamiltonian in free space without the trapping potential $m\omega^2 x^2/2$, while $\omega = \omega_z$ is an oscillation frequency in the axial direction. There is an inter-particle attraction between any two fermions with different quantum numbers.

In an elongated trap, the 1D effective coupling constant g_{1D} is related to the 3D scattering length a_{3D} . It is shown by Bergeman *et al.* [41, 42] that

$$g_{1D} = \frac{2\hbar^2 a_{3D}}{m a_\rho^2} \frac{1}{(1 - A a_{3D}/a_\rho)}, \quad (2.3)$$

where $a_\rho = \sqrt{\hbar/(m\omega_\rho)}$ is the characteristic oscillator length in the transverse axis. The constant $A = -\zeta(1/2)/\sqrt{2} \simeq 1.0326$ is responsible for a confinement induced Feshbach resonance [43], which changes the scattering properties dramatically when the 3D scattering length is comparable to the transverse oscillator length. It is convenient to express g_{1D} in terms of an effective 1D scattering length, $g_{1D} = -2\hbar^2/(ma_{1D})$, where

$$a_{1D} = -\frac{a_\rho^2}{a_{3D}} \left(1 - A \frac{a_{3D}}{a_\rho} \right) > 0. \quad (2.4)$$

Note that in this definition of the 1D scattering length, our sign convention is opposite to the 3D case.

In the homogeneous case, we measure the interactions by a dimensionless coupling constant γ , which is the ratio of the interaction energy density e_{int} to the kinetic energy density e_{kin} [37]. In the weak coupling, $e_{int} \sim g_{1D}n$ and $e_{kin} \sim \hbar^2 k^2/(2m) \sim \hbar^2 n^2/m$, where n is the total linear density of the gas. Therefore, one finds

$$\gamma = -\frac{mg_{1D}}{\hbar^2 n} = \frac{2}{na_{1D}}. \quad (2.5)$$

Thus, $\gamma \ll 1$ corresponds to the weakly interacting limit, while the strong coupling regime is realized when $\gamma \gg 1$.

B. Cluster states

In the case where all the fermions are distinct - which is only possible if the number of fermions is less than or equal to κ - the spatial wave-function can be completely symmetric. This allows one to construct eigenstates with identical symmetry to the exact solutions already known for a one-dimensional Bose gas with attractive interactions [44]. This exceptionally simple limiting case gives useful physical insight into the multi-particle clusters. These will be an essential feature in the physical properties of more general solutions. Accordingly, we may consider as a trial solution the localized quantum soliton state with wavefunction:

$$\Psi(x_1 \dots x_\kappa) = \exp \left\{ -c \sum_{i>j} |x_i - x_j| \right\} \quad (2.6)$$

On calculating the effect of the many-body Hamiltonian, we find that:

$$H_0 \Psi = E_\kappa \Psi + \left[\frac{2\hbar^2 c}{m} + g_{1D} \right] \left\{ \sum_{i>j} \delta(x_i - x_j) \right\} \Psi, \quad (2.7)$$

where the energy E_κ is:

$$E_\kappa = \frac{-\hbar^2 c^2 \kappa(\kappa^2 - 1)}{6m}. \quad (2.8)$$

This symmetric state with an asymptotic exponentially decaying wavefunction in each coordinate direction is the fundamental bound cluster. The requirement for this to be an eigenstate is simply:

$$c = \frac{-mg_{1D}}{2\hbar^2} = \frac{1}{a_{1D}} > 0. \quad (2.9)$$

In terms of this characteristic length-scale of $a_{1D} = 1/c$, one finds that the fundamental cluster binding energy can be written as:

$$\epsilon_B = \frac{\hbar^2 \kappa(\kappa^2 - 1)}{6ma_{1D}^2}. \quad (2.10)$$

These bound clusters can have either a fermionic or bosonic character, depending on whether κ is odd or even. The binding energy scales quadratically with the Hamiltonian coupling, and cubically with the number of bound fermions, κ . Clusters are localized relative to the center of mass, with a characteristic length scale of a_{1D} . One may reasonably expect some kind of physical transition to occur when the linear density exceeds $1/a_{1D}$, since at high density the Pauli exclusion principle will not allow independent clusters to form.

Thus, we can expect this type of symmetric bound state to predominate at low density, with a transition to a radically different behaviour at high density. This transition due to the Pauli exclusion principle is a unique feature of a 1D attractive Fermi gas, and does not occur in a 1D attractive Bose gas. By contrast, in an attractive Bose gas, clusters or quantum solitons can form with arbitrary particle number. They have been already observed with up to for $N = 10^7$ for photons in optical fibers [45], and $N = 10^3$ in the case of ultra-cold atoms [46]. However, clearly this is not to be expected in the case of fermions, where the spin multiplicity limits the size of this type of symmetric cluster.

For $\kappa = 3$, here is a close analogy between the symmetry properties of these bound clusters and the color symmetry properties of quark models in particle physics. In the case of quark matter, free nucleons are three-quark bound states. However, at high density, it is conjectured that there is a quantum phase-transition to a deconfined color superconductor state [23, 24]. This is expected physically at the core of massive neutron stars or in heavy-ion collisions. Although we are interested mainly in the one-dimensional case, we will show that a type of deconfining transition occurs here also.

C. Harmonic Trap

In the presence of a harmonic trap, we may characterize the interactions using the dimensionless coupling constant at the trap center γ_0 . For an ideal Fermi gas with equal spin population in each component, the total

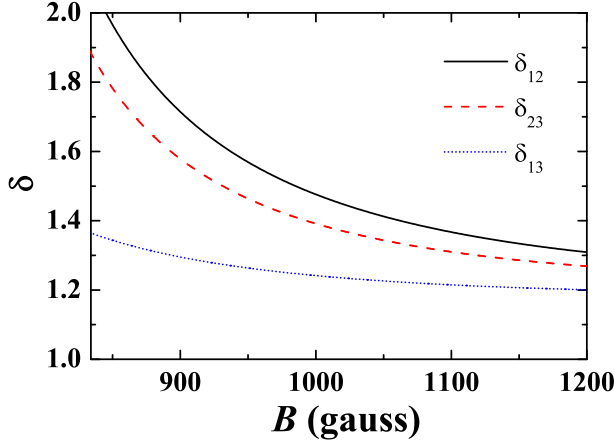


Figure 1: (Color online) One-dimensional interaction parameters for a three-component lithium gas in a two-dimensional optical lattice above the Feshbach resonances. Above a magnetic field $B = 1000$ Gauss, the difference of interaction parameters between different channels becomes very small, *i.e.*, $(\delta_{12} - \delta_{23})/\delta_{12} < 0.06$ and $(\delta_{12} - \delta_{13})/\delta_{12} < 0.16$. As a result, a three-component lithium gas can be well described by our exactly soluble model of 1D Fermi gases with a symmetric interaction.

linear density is

$$n_{ideal}(x) = n_{TF,\kappa}^0 \left[1 - \frac{x^2}{(x_{TF,\kappa}^0)^2} \right]^{1/2}, \quad (2.11)$$

in the large- N Thomas-Fermi (TF) limit, where

$$n_{TF,\kappa}^0 = \frac{(2N\kappa)^{1/2}}{\pi} a_{ho}^{-1}, \quad (2.12)$$

$$x_{TF,\kappa}^0 = \left(\frac{2N}{\kappa} \right)^{1/2} a_{ho}, \quad (2.13)$$

are the center linear density and the TF radius respectively. Here $a_{ho} = \sqrt{\hbar/(m\omega)}$ is the characteristic oscillator length in the axial direction. We therefore find that:

$$\gamma_0 = \left(\frac{2}{\kappa} \right)^{1/2} \pi \left[\frac{1}{N^{1/2}} \left(\frac{a_{ho}}{a_{1D}} \right) \right]. \quad (2.14)$$

To remove the dependence on the number of components κ , we define a dimensionless parameter

$$\delta = \left[N \frac{a_{1D}^2}{a_{ho}^2} \right]^{-1/2} \quad (2.15)$$

to describe the interactions. Note that the parameter δ depends inversely on the total number of particles. Hence, somewhat counter-intuitively, the gas becomes increasingly non-ideal with a decreasing number of atoms.

D. Parameter values

For experimental relevance, we now estimate interaction parameters for the on-going experiments on 1D lithium gases. Consider a gas of ^6Li atoms in 2D optical lattice with a typical lattice spacing periodicity $d = 532$ nm. The transverse oscillator length a_ρ is related to d via $a_\rho = d/(\pi s^{1/4})$ [47], where s is the ratio of the lattice depth to the recoil energy. Taking $s = 10$, this equation yields $a_\rho \simeq 95$ nm. Empirically, the 3D scattering length of ^6Li gases at these broad resonances is given by

$$a_{3d} = a_b[1 + W/(B - B_0)][1 + \alpha(B - B_0)]. \quad (2.16)$$

Detailed values of the background scattering length a_b , resonance position B_0 , resonance width W , and leading-order correction α have been measured precisely by Bartenstein *et al.* [27] for all three channels. As an example, we take a trapping frequency of $\omega = \omega_z = 2\pi \times 400$ Hz, which gives rise to $a_{ho} = 2052$ nm. The number of atoms in one tube of the lattice can be approximately of order $N \sim 100$. Given these parameters, we use Eqs. (2.4) and (2.15) to calculate δ . The estimated dimensionless coupling constants are shown in Fig. (1). Here, we focus on the BCS side of the resonances, and thus take a magnetic field $B > 834$ Gauss. We find that $\delta \sim O(1)$, *i.e.*, the gas is in an intermediate interacting regime. The difference in the interactions between different channels turns out to be small above 1000 Gauss. This justifies our choice of the same contact interaction potential between different hyperfine spin states.

III. HOMOGENEOUS MULTI-COMPONENT FERMION GASES

We first consider a uniform multi-component Fermi gas in one dimension with symmetric inter-component interactions. In this case, the model is exactly soluble via the Bethe ansatz [37, 38, 39, 40, 42, 48, 49, 50, 51, 52, 53]. For simplicity, we assume that each component has the same number of particles, *i.e.*, $N_l \equiv N/\kappa$ ($l = 1, 2, \dots, \kappa = 2S + 1$).

A. Ground State

In the ground state, the particles partition into groups of κ fermions. In each group, the fermions all have different quantum numbers, and are bound together to form a κ -body cluster. Introducing a linear number density, $n = N/L$, where L is the size of the system, the ground state energy E_{hom} in the thermodynamic limit is given by [40, 53],

$$\frac{E_{\text{hom}}}{L} = \frac{\hbar^2}{2m} \int_{-Q}^Q d\Lambda \left(\kappa \Lambda^2 - \frac{\kappa(\kappa^2 - 1)}{3} c^2 \right) \rho(\Lambda), \quad (3.1)$$

where the coupling $c = n\gamma/2 = 1/a_{1D}$ and $\rho(\Lambda)$ is the quasi-momentum distribution of κ -body clusters with a cut-off rapidity Q . The quasi-momentum distribution is determined by an integral equation [40, 53],

$$\rho(\Lambda) = \frac{\kappa}{2\pi} - \sum_{l=1}^{\kappa-1} \int_{-Q}^Q d\Lambda' \frac{2lc\rho(\Lambda')}{(2lc)^2 + (\Lambda - \Lambda')^2}, \quad (3.2)$$

and is normalized according to

$$n = \kappa \int_{-Q}^Q d\Lambda \rho(\Lambda), \quad (3.3)$$

which fix the value of the cut-off rapidity. The last term in E_{hom} is simply the contribution from κ -body bound states and is equal to $-(n/\kappa)\epsilon_{\kappa b}$, with binding energy identical to that given in the single-cluster result of Eq (2.10):

$$\epsilon_{\kappa b} \equiv \frac{\hbar^2}{2m} \frac{\kappa(\kappa^2 - 1)}{3} c^2 = \frac{\kappa(\kappa^2 - 1)}{6} \frac{\hbar^2}{ma_{1D}^2}. \quad (3.4)$$

We note that the binding energy of multi-component clusters increases rapidly with an increasing number of species κ . In particular, when $\kappa \geq 3$ it is larger than the pairing energy of $\kappa(\kappa - 1)/2$ Cooper pairs. In other words, if the binding energy was solely due to Cooper pairing, one would expect $\epsilon_{CP} = \kappa(\kappa - 1)\epsilon_{2b}/2$, where $\epsilon_{2b} = \hbar^2/ma_{1D}^2$ is the two-body binding energy. The increase above this level is due to κ -body correlations: κ particles interact more strongly with each in a cluster than as isolated pairs of particles.

B. Sound velocity

Once the ground state energy is obtained, we calculate the chemical potential $\mu_{\text{hom}} = \partial E_{\text{hom}}/\partial N$ and the corresponding sound velocity $c_{\text{hom}} = \sqrt{n(\partial\mu_{\text{hom}}/\partial n)/m}$. The sound velocity will be utilized later for predicting measurable collective mode frequencies. For numerical purposes, it is convenient to rewrite these in a dimensionless form that depends on the dimensionless coupling constant γ only,

$$\frac{E_{\text{hom}}}{L} \equiv \frac{\hbar^2 n^3}{2m} \left[e(\gamma) - \frac{(\kappa^2 - 1)}{12} \gamma^2 \right], \quad (3.5)$$

$$\mu_{\text{hom}} \equiv \frac{\hbar^2 n^2}{2m} \left[\mu(\gamma) - \frac{(\kappa^2 - 1)}{12} \gamma^2 \right], \quad (3.6)$$

$$c_{\text{hom}} \equiv \frac{\hbar n}{m} c(\gamma). \quad (3.7)$$

These are related by,

$$\mu(\gamma) = 3e(\gamma) - \gamma \frac{\partial e(\gamma)}{\partial \gamma}, \quad (3.8)$$

$$c(\gamma) = \mu(\gamma) - \frac{\gamma}{2} \frac{\partial \mu(\gamma)}{\partial \gamma}. \quad (3.9)$$

It is easy to see that for an ideal multi-component Fermi gas,

$$\frac{E_{\text{hom}}^{\text{ideal}}}{L} = \frac{\hbar^2 n^3}{2m} \left(\frac{\pi^2}{3\kappa^2} \right), \quad (3.10)$$

$$\mu_{\text{hom}}^{\text{ideal}} = \frac{\hbar^2 n^2}{2m} \left(\frac{\pi^2}{\kappa^2} \right), \quad (3.11)$$

$$c_{\text{hom}}^{\text{ideal}} = \frac{\hbar n}{m} \left(\frac{\pi}{\kappa} \right). \quad (3.12)$$

Therefore, as units of energy and sound velocity, we define a Fermi energy $\varepsilon_{F,\kappa} \equiv [\hbar^2 n^2/(2m)](\pi^2/\kappa^2)$ and a Fermi velocity $\nu_{F,\kappa} \equiv [\hbar n/m](\pi/\kappa)$.

C. Numerical solutions

The integral equation for the quasi-momentum distribution has to be solved numerically for a general coupling constant γ . To make it dimensionless, let us change variables as follows [37]:

$$\Lambda \equiv Qx; \quad 2c \equiv Q\lambda; \quad \rho(\Lambda) = g(x). \quad (3.13)$$

In terms of the new variables the quasi-momentum distribution, normalization condition, and ground state energy become, respectively,

$$\begin{aligned} g(x) &= \frac{\kappa}{2\pi} - \sum_{\ell=1}^{\kappa-1} \frac{\ell}{\pi} \int_{-1}^{+1} dx' \frac{\lambda g(x')}{(\ell\lambda)^2 + (x - x')^2}, \\ \lambda &= \kappa\gamma \int_{-1}^{+1} dx g(x), \\ e(\gamma) &= \frac{\gamma^3}{\lambda^3} \kappa \int_{-1}^{+1} dx x^2 g(x). \end{aligned} \quad (3.14)$$

To obtain better numerical accuracy for the chemical potential, it is useful to calculate the derivative of $e(\gamma)$ directly. With this goal, we introduce $\lambda_d = d\lambda/d\gamma$ and $g_d(x) = dg(x)/d\gamma$, which satisfy the coupled equations

$$\begin{aligned} g_d(x) &= - \sum_{\ell=1}^{\kappa-1} \frac{\ell}{\pi} \int_{-1}^{+1} dx' \left\{ \frac{\lambda g_d(x')}{(\ell\lambda)^2 + (x - x')^2} \right. \\ &\quad \left. - \frac{\lambda_d g(x) [-(\ell\lambda)^2 + (x - x')^2]}{[(\ell\lambda)^2 + (x - x')^2]^2} \right\}, \\ \lambda_d &= \frac{\lambda}{\gamma} + \kappa\gamma \int_{-1}^{+1} dx g_d(x). \end{aligned} \quad (3.15)$$

The derivative of $e(\gamma)$ is then obtained from

$$\frac{de}{d\gamma} = \frac{\gamma^3 \kappa}{\lambda^3} \int_{-1}^{+1} dx x^2 \left[\left(\frac{3}{\gamma} - \frac{3\lambda_d}{\lambda} \right) g_d(x) + g(x) \right]. \quad (3.16)$$

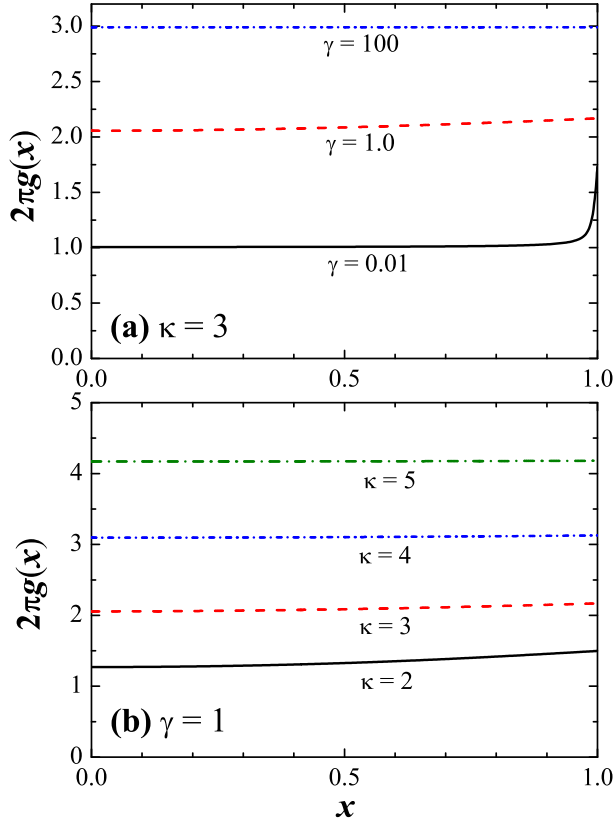


Figure 2: (Color online) Quasi-momentum distributions as a function of the dimensionless coupling constant (panel a) or as a function of the number of components (panel b). The distribution approaches to $\kappa/2\pi$ for a large interaction strength. While in the weak coupling limit, it goes to $1/(2\pi)$, but with a sharp increase at the boundary of $x = \pm 1$.

Numerically, the two set of integral equations, Eqs. (3.14) and Eqs. (3.15), have been solved by decomposing the integrals on a grid with $M = 1024$ points $\{x_i; x_i \in [-1, +1]\}$. For $g(x)$, we start from a set of trial distributions $g^{(0)}(x_i)$, with corresponding parameters of $\lambda^{(0)}$. Using the standard method for the integrals [37], we obtain a new distribution $g(x_i)$, and update λ accordingly. We iterate this procedure until $g(x_i)$ agrees with the previous distribution within a certain tolerance, and finally calculate the energy function $e(\gamma)$ using Eq. (3.14). The integral equation of $g_d(x)$ can be solved in the same manner, and finally Eq. (3.16) gives the derivative of the energy function $de/d\gamma$. We find that these iterative procedures for solving the integral equations are very stable. To obtain the sound velocity, the derivative of the chemical potential has been calculated accurately as a numerical derivative.

For an illustrative purpose, we show in Fig. (2) the quasi-momentum distribution function $g(x)$ as a function of the coupling constant (Fig. 2a) or as a function of the number of components (Fig. 2b). As $g(x)$ is an even function, we plot only the part with a positive x . For a large interaction strength, it approaches $\kappa/2\pi$, while in

the weak coupling limit, it reduces to $1/(2\pi)$. Below we discuss this limiting behavior in detail.

D. Strong coupling limit

For a strongly interacting or equivalently, a low density gas, in which the dimensionless coupling constant $\gamma \gg 1$, the value of λ in Eq (3.15) is extremely large. Thus, the integral kernel $l\lambda/\pi/[(l\lambda)^2 + (x-x')^2]$ becomes essentially a constant, $1/(\pi\ell\lambda)$. In addition, the quasi-momentum distribution function $g(x) \simeq g_0$. Then, the integral equation reduces to

$$g_0 = \frac{\kappa}{2\pi} - \sum_{\ell=1}^{\kappa-1} \left(\frac{1}{\ell}\right) \frac{2}{\pi\lambda} g_0. \quad (3.17)$$

At the same time, $\lambda = 2\kappa\gamma g_0$. Denoting $S_\kappa = (1/\kappa^2) \sum_{\ell=1}^{\kappa-1} \ell^{-1}$, we find that up to the order $1/\gamma^3$,

$$g(x) = \frac{\kappa}{2\pi} \left(1 - \frac{2S_\kappa}{\gamma}\right) + O\left(\frac{1}{\gamma^3}\right), \quad \gamma \rightarrow \infty. \quad (3.18)$$

Note that the factor S_κ decreases rapidly as the number of components increases, and goes like $S_\kappa \simeq \ln \kappa / \kappa^2$ when $\kappa \gg 1$. It is then straightforward to obtain that,

$$\begin{aligned} e(\gamma) &= \frac{\pi^2}{3\kappa^4} \left(1 + \frac{4S_\kappa}{\gamma} + \frac{12S_\kappa^2}{\gamma^2}\right), \\ \mu(\gamma) &= \frac{\pi^2}{\kappa^4} \left(1 + \frac{16S_\kappa}{3\gamma} + \frac{20S_\kappa^2}{\gamma^2}\right), \\ c(\gamma) &= \frac{\pi^2}{\kappa^4} \left(1 + \frac{8S_\kappa}{\gamma} + \frac{40S_\kappa^2}{\gamma^2}\right), \end{aligned} \quad (3.19)$$

and in dimensional form,

$$\begin{aligned} \frac{E_{\text{hom}}}{N} &= -\left(\frac{\epsilon_{\kappa b}}{\kappa}\right) + \frac{\hbar^2 n^2}{2m} \frac{\pi^2}{3\kappa^4} \left[1 + \frac{4S_\kappa}{\gamma} + \frac{12S_\kappa^2}{\gamma^2}\right], \\ \mu_{\text{hom}} &= -\left(\frac{\epsilon_{\kappa b}}{\kappa}\right) + \frac{\hbar^2 n^2}{2m} \frac{\pi^2}{\kappa^4} \left[1 + \frac{16S_\kappa}{3\gamma} + \frac{20S_\kappa^2}{\gamma^2}\right], \\ c_{\text{hom}} &= \frac{\hbar n}{m} \frac{\pi}{\kappa^2} \left[1 + \frac{8S_\kappa}{\gamma} + \frac{40S_\kappa^2}{\gamma^2}\right]^{1/2}. \end{aligned} \quad (3.20)$$

The first term on the right hand side of the total energy and chemical potential is simply the binding energy per particle of a 1D bound cluster from Eq (2.10), while the second term arises from interactions between clusters. These are strongly repulsive due to the Pauli exclusion principle between identical fermions. In the infinite coupling constant limit, the system behaves like a spinless Tonks-Girardeau gas of bound clusters with hard-core repulsive interactions. This is shown schematically in Fig (3).

Each cluster has a density n/κ and mass κm [54], giving rise to a chemical potential $\hbar^2 \pi^2 (n/\kappa)^2 / (2\kappa m) = [\hbar^2 / 2m] (\pi^2 / \kappa^3)$. This is exactly κ times the second term in the chemical potential μ_{hom} . It is worth emphasizing

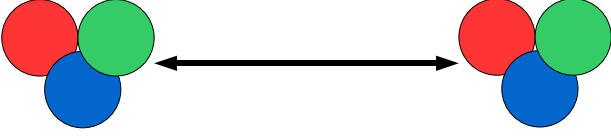


Figure 3: Schematic diagram of interacting bound clusters for $\kappa = 3$, in the low density limit.

that the compressibility of the system remains positive for $\gamma \rightarrow \infty$ as indicated by the first term in the sound velocity $c_{\text{hom}}, (\hbar n/m)(\pi/\kappa^2)$. This means that a 1D multi-component Fermi gas is mechanically stable, even in the strongly attractive regime. In contrast, the mechanical stability of a strongly interacting 3D multi-component gas with $\kappa \geq 3$ is not known exactly. It may experience collapse for sufficient large number of components, as suggested by Heiselberg [55]. For the stable, 1D case treated here, this low-density regime is analogous to the regime of isolated nucleons in QCD.

E. Weak coupling limit

The asymptotic behavior in the weak coupling limit is more subtle. Numerical calculation in the small γ limit suggests that $g(x) \rightarrow 1/(2\pi)$ and $\lambda \sim \gamma \rightarrow 0$. We then expand the quasi-momentum distribution,

$$g(x) = \frac{1}{2\pi} + f(x), \quad (3.21)$$

where $f(x) = O(\gamma) \ll 1$ satisfies,

$$f(x) = \frac{\kappa-1}{2\pi} - \sum_{\ell=1}^{\kappa-1} \frac{\ell}{\pi} \int_{-1}^{+1} dx' \frac{\lambda}{(\ell\lambda)^2 + (x-x')^2} \frac{1}{2\pi} \\ - \sum_{\ell=1}^{\kappa-1} \frac{\ell}{\pi} \int_{-1}^{+1} dx' \frac{\lambda}{(\ell\lambda)^2 + (x-x')^2} f(x). \quad (3.22)$$

As $\lambda \rightarrow 0$, to the leading order $\ell\lambda/\pi/[(\ell\lambda)^2 + (x-x')^2] \simeq \delta(x-x')$. Thus,

$$f(x) = \frac{1}{2\pi\kappa} \left[\kappa - 1 - \sum_{\ell=1}^{\kappa-1} \int_{-1}^{+1} \frac{dx' (\ell\lambda/\pi)}{(\ell\lambda)^2 + (x-x')^2} \right]. \quad (3.23)$$

For small λ , the integral in $f(x)$ is well approximated by,

$$\frac{\ell}{\pi} \int_{-1}^{+1} dx' \frac{\lambda}{(\ell\lambda)^2 + (x-x')^2} \simeq 1 - \frac{2}{\pi} \frac{\ell\lambda}{1-x^2}. \quad (3.24)$$

We find then to the order of γ ,

$$f(x) = \frac{\kappa-1}{2\pi^2} \frac{\lambda}{1-x^2}, \quad (3.25)$$

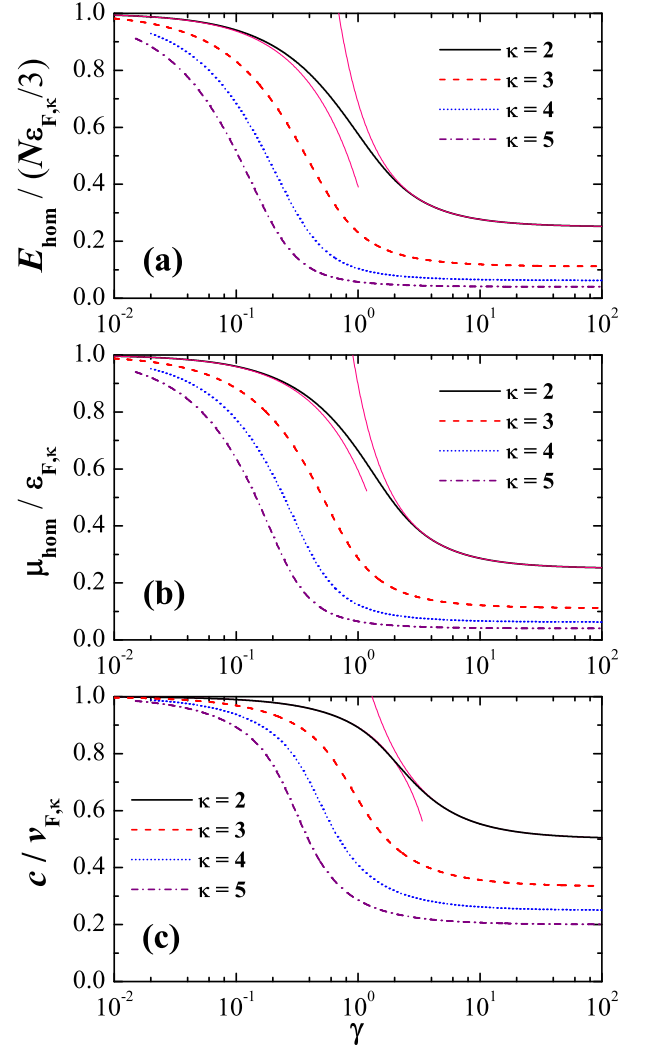


Figure 4: (Color online) Dependence of the uniform ground state energy per particle (a), the chemical potential (b), and the velocity of sound (c) on the dimensionless coupling constant γ , at several number of species as indicated. The energy and sound velocity are in units of the Fermi energy $\varepsilon_{F,\kappa} \equiv [\hbar^2 n^2/(2m)](\pi^2/\kappa^2)$ and the Fermi velocity $v_{F,\kappa} \equiv [\hbar n/m](\pi/\kappa)$, respectively. Thin solid lines are the analytic results in the two limiting cases for $\kappa = 2$, as described in Eq. (3.20) and Eq. (3.29).

which diverges at the boundary $x = \pm 1$. It is straightforward to show that,

$$\int_{-1}^{+1} dx g(x) = \frac{1}{\pi} - \frac{\kappa-1}{2\pi^2} \lambda \ln \lambda + \dots \quad (3.26)$$

$$\int_{-1}^{+1} dx (1-x^2) g(x) = \frac{2}{3\pi} + \frac{\kappa-1}{\pi^2} \lambda + \dots \quad (3.27)$$

Substituting these results into the energy function

$e(\gamma)$, it is easy to obtain,

$$e(\gamma) = \frac{\pi^2}{3\kappa^2} - \frac{\pi(\kappa-1)}{\kappa^2}\lambda - \frac{(\kappa-1)^2}{4\kappa^2}\lambda^2 \ln^2 \lambda. \quad (3.28)$$

Recall that $\lambda = \kappa\gamma \int_{-1}^{+1} g(x) \approx \kappa\gamma/\pi$. The equation of state and the sound velocity are finally given by,

$$\begin{aligned} \frac{E_{\text{hom}}}{N} &= \frac{\hbar^2 n^2}{2m} \left[\frac{\pi^2}{3\kappa^2} - \frac{(\kappa-1)}{\kappa}\gamma - \frac{(\kappa-1)^2}{4\pi^2}\gamma^2 \ln^2 \gamma \right], \\ \mu_{\text{hom}} &= \frac{\hbar^2 n^2}{2m} \left[\frac{\pi^2}{\kappa^2} - 2\frac{(\kappa-1)}{\kappa}\gamma - \frac{(\kappa-1)^2}{4\pi^2}\gamma^2 \ln^2 \gamma \right], \\ c_{\text{hom}} &= \frac{\hbar n}{m} \frac{\pi}{\kappa} \left[1 - \frac{\kappa(\kappa-1)}{\pi^2}\gamma \right]^{1/2}, \end{aligned} \quad (3.29)$$

where the first terms on the right hand side are identical to an ideal (non-interacting) multi-component Fermi gas, as one might expect. Note that the binding energy of bound clusters is of second order in γ , and therefore is not included in the above expressions. Two-body correlations are dominant in the weakly interacting limit, and give rise to the mean-field Hartree-Fock attractive corrections in the second term on the right hand side. The non-perturbative terms of order $\gamma^2 \ln^2 \gamma$ are beyond mean-field theory. This regime is analogous to the color-superconductor regime expected in quark matter.

F. Numerical results

In Fig. (4), we give the equation of state and the sound velocity as a function of the dimensionless coupling constant γ , obtained by numerically solving the integral equations. The ground state energy per particle and the chemical potential are measured in units of one-third of the Fermi energy and the Fermi energy, respectively, while the sound velocity is in units of the Fermi velocity. We consider a number of components ranging up to $\kappa = 5$ to show the overall trend.

Starting from the ideal gas results, the thermodynamic and dynamic quantities decrease with increasing coupling constant, and finally saturate to the Tonk-Girardeau (repulsive) gas limit, as already anticipated. The rate of decrease is much faster as the number of components κ increases. This implies that the gas becomes more attractive when the number of particles in the bound cluster increases. We show also in the figure the asymptotic behavior in the two limiting cases for $\kappa = 2$ by thin solid lines. These fit fairly well with the full numerical results, apart from a small intermediate interaction region about $\gamma \sim 1$.

IV. MULTI-COMPONENT TRAPPED FERMION GAS

To make quantitative contact with on-going experiments, it is crucial to take into account the external har-

monic trapping potential $V_{\text{trap}}(x) = m\omega^2 x^2/2$, which is necessary to prevent the fermions from escaping. For a large number of fermions, which is likely to be $N \sim 100$ experimentally, an efficient way to take the trap into account is by using the local density approximation (LDA). Together with the exact homogeneous equation of state of a 1D multi-component Fermi gas, this gives an asymptotically exact results as long as $N \gg 1$.

The basic idea of the LDA is that an inhomogeneous gas of large size can be treated locally as infinite matter with a local chemical potential. We may then partition the cloud into many blocks, in each of which the number of fermions is much greater than unity. Provided the variation of the trap potential across each block is negligible compared with the local Fermi energy, any interface effects may be safely neglected. Thus, each block is un-correlated with the others. We note that in 1D the interface energy scales as N^{-1} compared to the total energy, and thus the LDA becomes valid provided $N \gg 1$.

In detail, the LDA amounts to determining the chemical potential μ from the local equilibrium condition [42, 48, 49],

$$\mu_{\text{hom}}[n(x)] + \frac{1}{2}m\omega^2 x^2 = \mu_g, \quad (4.1)$$

under the normalization restriction,

$$N = \int_{-x_{TF}}^{+x_{TF}} n(x) dx, \quad (4.2)$$

where $n(x)$ is the total linear number density and is nonzero inside a Thomas-Fermi radius x_{TF} . We have used the subscript “g” to distinguish the global chemical potential μ_g from the local chemical potential μ_{hom} . Rewriting μ_{hom} into the dimensionless form $\mu[\gamma(x)]$, where $\gamma(x) = 2/[n(x)a_{1D}]$, we find that

$$-\frac{(\kappa^2-1)\hbar^2}{6ma_{1D}^2} + \frac{\hbar^2 n^2(x)}{2m} \mu[\gamma(x)] + \frac{1}{2}m\omega^2 x^2 = \mu_g. \quad (4.3)$$

The first term on the left hand side is simply the binding energy, and causes a constant shift to the chemical potential. To solve the LDA equations, it is simplest to transform into a dimensionless form, by defining

$$\tilde{\mu}_g = \mu_g \frac{ma_{1D}^2}{\hbar^2} + \frac{(\kappa^2-1)}{6}, \quad (4.4)$$

$$\tilde{x} = \frac{a_{1D}x}{a_{ho}^2}, \quad (4.5)$$

$$\tilde{n} = na_{1D}, \quad (4.6)$$

where the binding energy is now absorbed in the redefinition of chemical potential. Thus, the local equilibrium condition becomes,

$$\frac{\tilde{n}^2(\tilde{x})}{2} \mu[\gamma(\tilde{x})] + \frac{\tilde{x}^2}{2} = \tilde{\mu}_g, \quad (4.7)$$

where the dimensionless coupling constant now takes the form, $\gamma(\tilde{x}) = 2/\tilde{n}(\tilde{x})$. Accordingly, the normalization condition is given by

$$\int_{-\tilde{x}_{TF}}^{+\tilde{x}_{TF}} d\tilde{x} \tilde{n}(\tilde{x}) = N \frac{a_{1D}^2}{a_{ho}^2} = \frac{1}{\delta^2}, \quad (4.8)$$

where δ is the interaction parameter for a trapped gas defined earlier in Eq. (2.15). It is clear that the LDA equations are controlled by a single parameter δ : $\delta \ll 1$ corresponds to the weakly coupling limit, while $\delta \gg 1$ corresponds to the strongly interacting regime.

The numerical procedure of solving the LDA equations is straightforward. For a given interaction parameter δ , and initial guess for $\tilde{\mu}_g$, we invert the dimensionless local equilibrium equations to find $\gamma(\tilde{x})$ and the linear density $\tilde{n}(\tilde{x}) = 2/\gamma(\tilde{x})$. The chemical potentials $\tilde{\mu}_g$ are then adjusted to enforce the number conservation, giving a better estimate for the next iterative step. The iteration is continued until the number normalization condition is satisfied within a certain range.

A. Density profiles and the equation of state

The asymptotic behavior of density profiles can be determined analytically in the strong and weak coupling limits. In the strong interaction regime of $\delta \gg 1$, $\mu(\gamma) = (\pi^2/\kappa^4)[1 + 16S_\kappa/(3\gamma)]$, and the local equilibrium condition is given by,

$$\frac{\tilde{n}^2(\tilde{x})}{2} \frac{\pi^2}{\kappa^4} \left[1 + \frac{16S_\kappa}{3\gamma(\tilde{x})} \right] + \frac{\tilde{x}^2}{2} = \tilde{\mu}_g. \quad (4.9)$$

In the infinite coupling limit of Tonks-Girardeau gas, where $\gamma(\tilde{x}) \rightarrow \infty$ and therefore the second term in $\mu(\gamma)$ vanishes, the density profile takes the form,

$$\tilde{n}_{TG}(\tilde{x}) = \frac{\sqrt{2}\kappa}{\pi\delta} \left(1 - \frac{\kappa^2\delta^2}{2}\tilde{x}^2 \right)^{1/2}, \quad (4.10)$$

and the global chemical potential is,

$$\tilde{\mu}_g^{(0)} = \frac{1}{\kappa^2\delta^2}. \quad (4.11)$$

The inclusion of the next order of $1/\gamma$ in $\mu(\gamma)$ leads to a density variation $\Delta\tilde{n}(\tilde{x})$, as well as a change in the chemical potential $\Delta\tilde{\mu}_g$. Linearizing the local equilibrium condition, we find that,

$$\Delta\tilde{n}(\tilde{x}) = \frac{\kappa^4}{\pi^2} \frac{\Delta\tilde{\mu}_g}{\tilde{n}_{TG}(\tilde{x})} - \frac{8S_\kappa}{3} [\tilde{n}_{TG}(\tilde{x})]^2. \quad (4.12)$$

Number conservation $\int d\tilde{x} \Delta\tilde{n}(\tilde{x}) = 0$ yields,

$$\Delta\tilde{\mu}_g = \frac{64\sqrt{2}S_\kappa}{9\pi^2\kappa\delta^3}. \quad (4.13)$$

Restoring the equations to dimensional form, the density profile of a strongly interacting gas becomes,

$$n(x)_{\delta \gg 1} = n_{TG}(x) + \Delta n(x), \quad (4.14)$$

where

$$n_{TG}(x) = \sqrt{\kappa} n_{TF,\kappa}^0 \left[1 - \frac{\kappa x^2}{(x_{TF,\kappa}^0)^2} \right]^{1/2}, \quad (4.15)$$

is the profile of a spinless Tonks-Girardeau gas, and the density variation,

$$\Delta n(x) = \frac{32\sqrt{2}\kappa^{3/2}S_\kappa}{9\pi^2\delta} n_{TF,\kappa}^0 \left\{ \left[1 - \frac{\kappa x^2}{(x_{TF,\kappa}^0)^2} \right]^{-1/2} - \frac{3\pi}{4} \left[1 - \frac{\kappa x^2}{(x_{TF,\kappa}^0)^2} \right] \right\}. \quad (4.16)$$

Accordingly, the chemical potential takes the form,

$$\mu_g^{\delta \gg 1} = -\frac{(\kappa^2 - 1)\hbar^2}{6ma_{1D}^2} + \frac{N\hbar\omega}{\kappa^2} \left[1 + \frac{64\sqrt{2}\kappa S_\kappa}{9\pi^2} \frac{1}{\delta} \right]. \quad (4.17)$$

where the first term on the right hand side is again from the binding energy, while the second term corresponds to the chemical potential of a spinless Tonks-Girardeau gas of bound clusters. For later reference, we calculate the mean-square size of the cloud $\langle x^2 \rangle = \int dx x^2 n(x)/N$ using the strongly interacting density profile $n(x)_{\delta \gg 1}$, and find that,

$$\langle x^2 \rangle_{\delta \gg 1} = \frac{N}{2\kappa^2} a_{ho}^2 + \frac{32\sqrt{2}S_\kappa}{15\pi^2\kappa} N^{3/2} a_{1D} a_{ho}. \quad (4.18)$$

The density profile of a weakly interacting gas can be calculated in the same manner. The leading order contribution is simply the ideal gas result, $n_{ideal}(x)$, and the Hartree-Fock correction to the chemical potential gives rise to a density variation which is proportional to the interaction strength g_{1D} . Explicitly, we find that,

$$n(x)_{\delta \ll 1} = n_{ideal}(x) + \Delta n(x), \quad (4.19)$$

where

$$\Delta n(x) = \frac{2\kappa(\kappa - 1)}{\pi^2 a_{1D}} \left[1 - \frac{2/\pi}{\sqrt{1 - x^2/(x_{TF,\kappa}^0)^2}} \right]. \quad (4.20)$$

The chemical potential is given by,

$$\mu_g^{\delta \ll 1} = \frac{N\hbar\omega}{\kappa} \left[1 - \frac{4\sqrt{2}\kappa(\kappa - 1)}{\pi^2} \delta \right]. \quad (4.21)$$

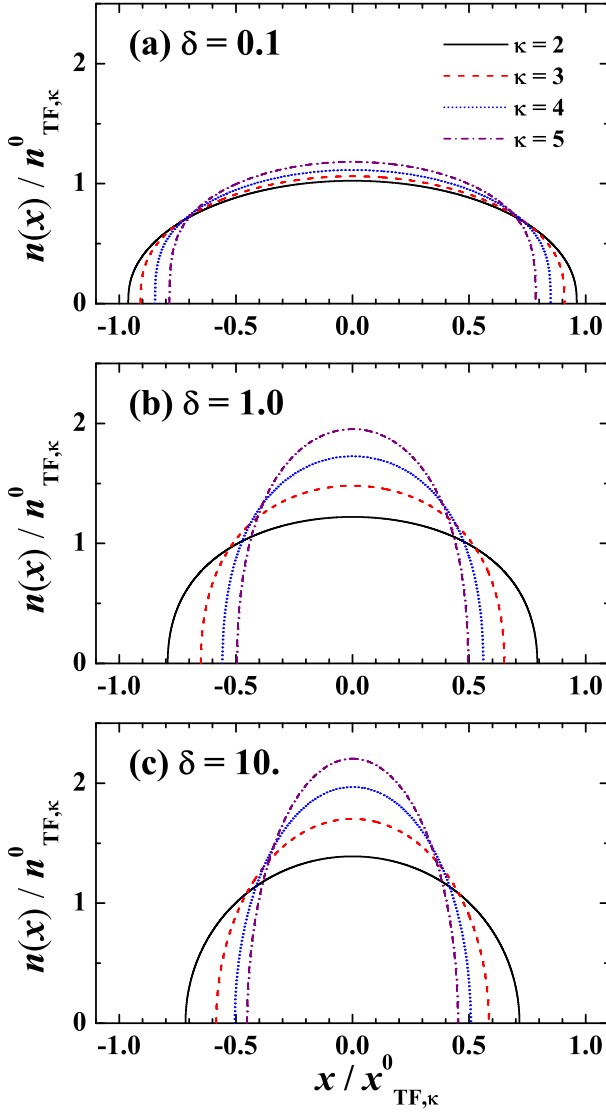


Figure 5: (Color online) Density profiles of a 1D trapped multi-component Fermi cloud at three interaction parameters $\delta = 0.1$ (a), $\delta = 1.0$ (b), and $\delta = 10$ (c). The linear density and the coordinate are in units of the peak density $n_{TF,\kappa}^0$ and Thomas-Fermi radius $x_{TF,\kappa}^0$ of an ideal gas, respectively.

The mean-square size of the cloud is found to be,

$$\langle x^2 \rangle_{\delta \ll 1} = \frac{N}{2\kappa} a_{ho}^2 - \frac{4}{3} \sqrt{\frac{2}{\kappa}} \frac{\kappa - 1}{\pi^2} N^{1/2} \frac{a_{ho}^3}{a_{1D}}. \quad (4.22)$$

Fig. (5) plots numerical results for the density profiles at three interaction parameters and at different number of species as indicated. The linear density and the coordinate are in units of the peak density $n_{TF,\kappa}^0$ and Thomas-Fermi radius $x_{TF,\kappa}^0$ of an ideal gas, respectively. With increasing interaction parameter δ (from Figs. (5a) to (5c)), the density profiles change from an ideal gas distribution to a strongly interacting Tonk-Girardeau profile. At the same interaction parameter, the density profiles become sharper and narrower as the number of species

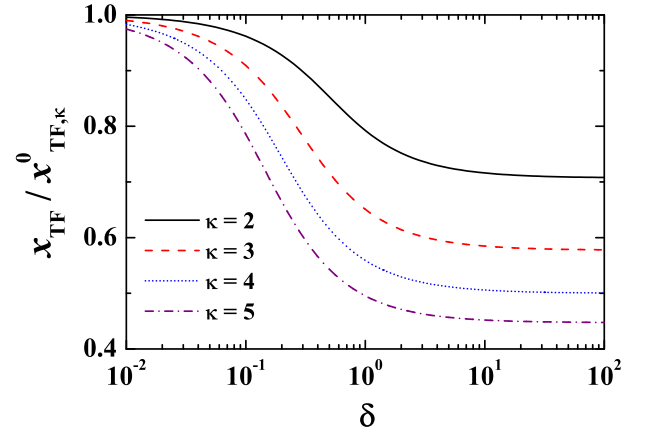


Figure 6: (Color online) Thomas-Fermi radius, in units of $x_{TF,\kappa}^0$, as a function of the interaction parameter, at several number of component as indicated.

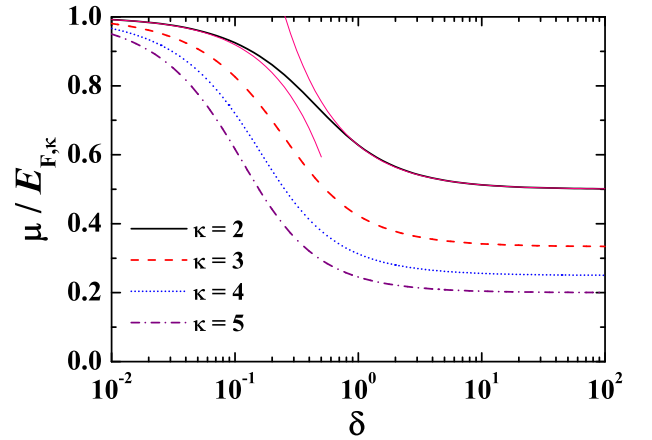


Figure 7: (Color online) Chemical potential as a function of the interaction parameter δ . It is in units of $E_{F,\kappa} = N\hbar\omega/\kappa$. Thin solid lines are the analytic results in the two limiting cases for $\kappa = 2$, as described in Eqs. (4.17) and (4.21).

κ increases. We display also the Thomas-Fermi radius of the cloud in Fig. (6) as a function of the interaction strength. It decreases monotonically from the ideal gas result $x_{TF,\kappa}^0$ to the Tonk-Girardeau prediction $x_{TF,\kappa}^0/\sqrt{\kappa}$ as the interaction parameter increases, thus increasing the compressive force of the attractive interactions.

Fig. (7) reports the dependence of the chemical potential on the interaction strength, at several numbers of species as indicated. Here, for clarity we have subtracted the binding energy part of the chemical potential. For $\kappa = 2$, we show the asymptotic behavior given by Eqs. (4.17) and (4.21) by thin solid lines. They fit very well with the numerical results, except at the intermediate interaction regime.

B. Low-lying collective modes

Experimentally, a useful way to characterize an interacting system is to measure its low-lying collective excitations of density oscillations. For a uniform gas, the low-lying collective excitations are simply the sound waves with energy $\Omega(k) = c|\mathbf{k}|$ for a given momentum $k < k_F$, which is gapless as $k \rightarrow 0$. In traps, however, the spectrum becomes discrete, due to the finite cloud size of the gas that is of order $x_{TF,\kappa}^0$. There is a minimum value of the momentum $k_{\min} \sim 1/x_{TF,\kappa}^0$. Taking a sound velocity at the trap center $c \sim (\hbar n_{TF,\kappa}^0/m)(\pi/\kappa)$, one finds that,

$$\Omega(k_{\min}) \sim \frac{\hbar n_{TF,\kappa}^0}{m} \frac{\pi}{\kappa} \frac{1}{x_{TF,\kappa}^0} = \omega, \quad (4.23)$$

comparable to the energy level of the harmonic trap.

Quantitative calculations of the low-lying collective excitations in traps can be based on the superfluid hydrodynamic description of the dynamics of the 1D Fermi gas [56]. In such a description, the density $n(x, t)$ and the velocity field $v(x, t)$ satisfy the equation of continuity

$$\frac{\partial n(x, t)}{\partial t} + \frac{\partial}{\partial x} [n(x, t) v(x, t)] = 0, \quad (4.24)$$

and the Euler equation

$$m \frac{\partial v}{\partial t} + \frac{\partial}{\partial x} \left[\mu_{\text{hom}}(n) + V_{\text{trap}}(x) + \frac{1}{2} m v^2 \right] = 0. \quad (4.25)$$

We consider the fluctuations of the density and the velocity field about the equilibrium ground state, $\delta n(x, t) = n(x, t) - n(x)$ and $\delta v(x, t) = v(x, t) - v(x) = v(x, t)$, where $n(x)$ and $v(x) \equiv 0$ are the equilibrium density profile and velocity field. Linearizing the hydrodynamic equations, one finds that [56],

$$\frac{\partial^2}{\partial t^2} \delta n(x, t) = \frac{1}{m} \frac{\partial}{\partial x} \left\{ n \frac{\partial}{\partial x} \left[\frac{\partial \mu_{\text{hom}}(n)}{\partial n} \delta n(x, t) \right] \right\}. \quad (4.26)$$

The boundary condition requires that the current $j(x, t) = n(x) \delta v(x, t)$ should vanish identically at the Thomas-Fermi radius $x = \pm x_{TF}$. Considering the n th eigenmode with $\delta n(x, t) = \delta n(x) \exp[i\omega_n t]$ and removing the time-dependence, we end up with an eigenvalue problem, *i.e.*,

$$\frac{1}{m} \frac{d}{dx} \left\{ n \frac{d}{dx} \left[\frac{\partial \mu_{\text{hom}}(n)}{\partial n} \delta n(x) \right] \right\} + \omega_n^2 \delta n(x) = 0. \quad (4.27)$$

We develop a powerful multi-series-expansion method to solve the above 1D hydrodynamics equation, as outlined in detail in the Appendix. The resulting low-lying collective mode can be classified by the number of nodes in its eigenfunction, *i.e.*, the number index “ n ”. The lowest two modes with $n = 1, 2$ have very transparent physical meaning. These are respectively the dipole and breathing (compressional) modes, which can be excited

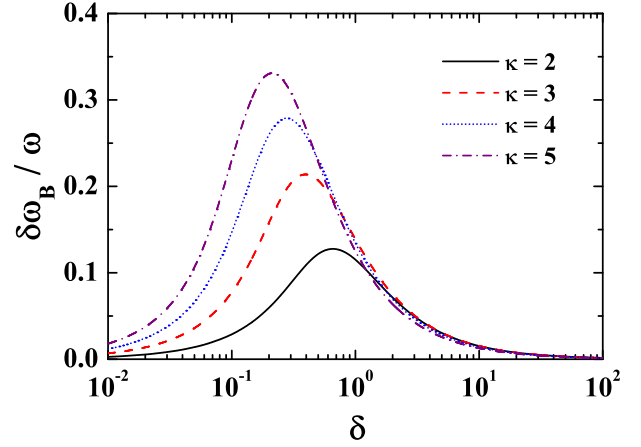


Figure 8: (Color online) Frequency corrections (with respect to the ideal gas value) of the lowest breathing modes $\delta\omega_B$ as a function of the dimensionless coupling parameter δ , at several number of species as indicated.

separately by shifting the trap center or modulating the harmonic trapping frequency. The dipole mode is not affected by interactions according to Kohn’s theorem, and has an invariant frequency precisely at $\omega_1 = \omega$.

The low-lying hydrodynamic modes of a two-component Fermi gas in the weak and strong coupling limits have been discussed analytically by Minguzzi [57]. In both limits, the cloud behaves like a spinless ideal Fermi gas. Therefore, the frequency ω_n of the mode “ n ” is fixed to $n\omega$. This result applies to a multi-component 1D Fermi gas as well.

Fig. (8) shows the interaction dependence of frequencies of the breathing mode for a multi-component gas with different numbers of components. Here, to stress the role of interactions, the deviation of the mode frequency from its ideal result, $\delta\omega_B = \omega_B - \omega$, has been plotted. As a function of the interaction parameter, a peak in $\delta\omega_B$ emerges at the intermediate interaction regime $\delta \sim 1$. The peak value increases with increasing the number of components κ . This peak is a clear signature of the cross-over from a regime of multi-particle clusters to a color quasi-superconductor.

Fig. (9) shows the frequency correction $\delta\omega_n = \omega_n - n\omega$ of the low-lying modes of a three-component gas as a function of the interaction strength. The dipole mode frequency is always ω , as expected, while all other modes show a non-trivial peak structure, similar to that of the breathing mode. It is evident that the higher mode index “ n ” is, the larger frequency correction.

As an alternative to the numerical solution of the 1D hydrodynamic equation, the frequency of the breathing mode may be obtained by applying the compressibility sum-rule. As long as the breathing mode exhausts all the weights in the dynamic structure factor, the mode

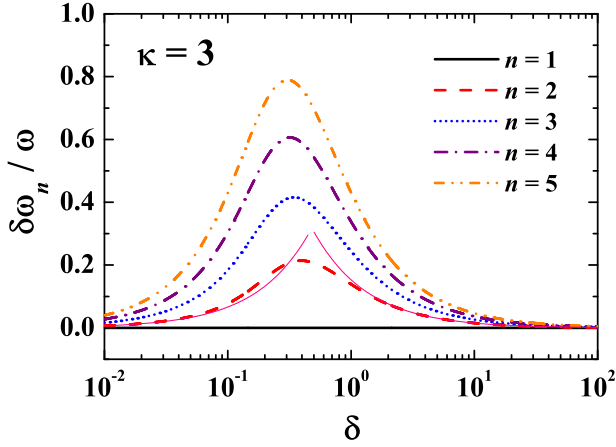


Figure 9: (Color online) Interaction strength dependence of the frequency corrections $\delta\omega_n = \omega_n - n\omega$ of the low-lying collective modes of a 1D three-component Fermi gas. Thin solid lines are the analytic sum-rule expansions for the weakly and strongly interacting limits, as described in Eqs. (4.29) and (4.30), respectively.

frequency can be calculated according to [42, 56],

$$\omega_B^2 = -2 \frac{\langle x^2 \rangle}{d\langle x^2 \rangle / d\omega^2}. \quad (4.28)$$

We have performed such calculations. The resulting frequency agrees extremely well with that from solving the 1D hydrodynamic equation, with a relative difference less than 10^{-4} . Such a good agreement gives strong support to the application of the sum-rule. To gain further insight of the breathing mode frequency, we use the sum-rule to obtain analytically the first order correction to the frequency for the weak and strong coupling limits. This can be done by substituting the expression for the mean-square size of the cloud in Eqs. (4.18) and (4.22) into the sum-rule formalism (4.28). Replacing $a_{ho} = \sqrt{\hbar/m\omega}$ and taking the derivative with respect to ω^2 , we find that

$$\omega_B^{\delta \gg 1} = 2\omega \left(1 + \frac{16\sqrt{2}\kappa S_\kappa}{15\pi^2} \frac{1}{\delta} \right), \quad (4.29)$$

for the strongly interacting limit, and

$$\omega_B^{\delta \ll 1} = 2\omega \left[1 + \frac{2\sqrt{2}\kappa(\kappa-1)}{3\pi^2} \delta \right], \quad (4.30)$$

for the weak coupling regime. Thin solid lines in Fig. (9) show the resulting analytic expansions for $\delta\omega_B$ for a three-component Fermi gas. These expansions describe very well the breathing mode frequency over a fairly large range of interaction strengths, but break down at the intermediate coupling regime $\delta \sim 1$.

V. CONCLUSION

In conclusion, we have investigated the properties of 1D attractive multi-component Fermi gases, based on the Bethe ansatz exact solution, in a homogeneous environment. This was extended to include a harmonic trap, by using the local density approximation. The equation of state of the system has been discussed in detail, as well as some dynamical quantities, including the sound velocity and low-lying collective modes.

We have drawn attention to the formation of multi-body bound clusters, which are always present in a 1D attractive multi-component gas. These clusters are not well understood, as their description is beyond the mean-field theory. We have found that such multi-body clusters have significant impact on the equation of state and dynamic behavior of the systems. In particular, as the number of particles in the clusters increase, the gas turns out to be increasingly attractive compared to a simple Cooper-pairing scenario. This is suggestive of the strongly interacting nature of the bound clusters.

There is a close analogy between the proposed properties of QCD at high density, and the results we calculate for a three-component Fermi gas in 1D. In both cases there is a transition between discrete multi-particle clusters (nucleons) to a coherent quasi-superfluid (colour superconductor), as the density increases. For the 1D case, both the high and low density limits result in free particle dynamics, with different multiplicities. This gives simple collective mode behaviour in either limit. However, the transition region with $\gamma \simeq 1$ can show very strong evidence of a transition. This is due to an easily observed peak in the collective breathing mode frequency.

Our results should be useful for on-going experiments on 1D multi-component atomic Fermi gases. An example of particular interest is three-component lithium gas, which has three broad Feshbach resonances. Our estimate of the relevant parameters suggests that an ultra-cold gas of ^6Li atoms in an optical lattice, above a magnetic field $B = 1000$ Gauss, can be nearly described by the current model. Our prediction of the density profiles and low-lying collective modes, provide a useful characterization of an interacting 1D three-component Fermi gas. We expect this to be testable in a future experiment.

Acknowledgments

This work was supported by the Australian Research Council Center of Excellence, the National Natural Science Foundation of China Grants Nos. NSFC-10574080 and NSFC-10774190, and the National Fundamental Research Program of China Grants Nos. 2006CB921404 and 2006CB921306.

Appendix

In this appendix, we outline the procedure of solving the 1D hydrodynamic equation,

$$\frac{1}{m} \frac{d}{dx} \left\{ n \frac{d}{dx} \left[\frac{\partial \mu_{\text{hom}}(n)}{\partial n} \delta n(x) \right] \right\} + \omega_n^2 \delta n(x) = 0, \quad (5.1)$$

with the boundary condition that the current $j(x) \propto \partial_x \{ \delta n(x) \partial \mu_{\text{hom}}[n(x)] / \partial n(x) \}$ must vanish at $x = \pm x_{TF}$.

It is convenient to introduce a function,

$$f(x) \equiv \frac{\partial \mu_{\text{hom}}[n(x)]}{\partial n(x)} \delta n(x), \quad (5.2)$$

and rewrite the hydrodynamic equation in the form,

$$x \frac{d^2 f}{dx^2} + x \frac{d \ln[n(x)]}{dx} \frac{df}{dx} + \left(\frac{\omega_m}{\omega} \right)^2 \frac{\omega^2 x}{c^2(x)} f = 0, \quad (5.3)$$

where $c(x) = [n(x) \partial \mu_{\text{hom}}[n(x)] / \partial n(x) / m]^{1/2}$ is the local sound velocity at position x . Let us introduce $A(x) \equiv \ln[n(x)]$, $A_1(x) \equiv -\omega^2 x / c^2(x)$, and $\nu_m \equiv \omega_m / \omega$. Then the above equation becomes,

$$x \frac{d^2 f}{dx^2} + x \frac{dA}{dx} \frac{df}{dx} - \nu_m^2 A_1(x) f = 0. \quad (5.4)$$

Here the variable $x \in [-x_{TF}, +x_{TF}]$. Note that for our specific case, $A_1(x) = dA(x)/dx$, due to the local equilibrium condition.

To solve the equation, one may wish to change x to a new variable $y \in [0, 1]$. This can be done by two steps. First, we define $f(x) \equiv x^l v(x)$, where $l = 0$ or 1 corresponds to the parity of the modes. Translating to $v(x)$, we have (now $x \in [0, +x_{TF}]$),

$$x \frac{d^2 v}{dx^2} + \left(2l + x \frac{dA}{dx} \right) \frac{dv}{dx} - \left[\nu_m^2 A_1 - l \frac{dA}{dx} \right] v = 0. \quad (5.5)$$

At the second step, we define $y \equiv (x/x_{TF})^2$ and change to the new variable y . After some straightforward calculations, we obtain the following equation for $v(y)$,

$$y(1-y)^2 \frac{d^2 v}{dy^2} + (1-y)^2 \left[\Delta + y \frac{dA}{dy} \right] \frac{dv}{dy} + \frac{1}{2} (1-y)^2 \left[l \frac{dA}{dy} - \nu_m^2 \tilde{A}_1(y) \right] v = 0, \quad (5.6)$$

where $\Delta \equiv l + 1/2$ and $\tilde{A}_1(y) \equiv A_1(y) / (2y^{1/2})$. In practise, the value of dA/dy can be calculated as follows,

$$\frac{dA}{dy} \equiv -\frac{m\omega^2 x_{TF}^2}{2} \left[\frac{1}{n \partial \mu_{\text{hom}}[n] / \partial n} \right]_{n=n(x=x_{TF}\sqrt{y})}. \quad (5.7)$$

Note that in our case $\tilde{A}_1(y) = dA/dy$. Here, we multiply a factor of $(1-y)^2$ on both sides of Eq. (5.6), in order to remove the singularity of dA/dy and $\tilde{A}_1(y)$ at point $y = 1$.

We develop a multi-series-expansion method to solve the eigenvalue problem Eq. (5.6). As the current vanishes at the Thomas-Fermi boundary, the eigenfunction of Eq. (5.6) should not be singular at $y = 1$. As well, we require that the eigenfunction has to take a finite value at $y = 0$. As we shall see, these two boundary conditions give rise to a set of the discrete spectrum, as well as a complete set of the eigenfunctions.

To apply the boundary conditions, we divide the whole region $[0, 1]$ into many pieces, for example, M parts, $[0, 1] = [y_0 = 0, y_1] \cup [y_1, y_2] \cup \dots \cup [y_{M-1}, y_M = 1]$. We look for the solution in the form,

$$v(y) = \sum_{n=0}^{\infty} a_{in} (y - y_i)^n, \quad \text{if } y \in [y_i, y_{i+1}]. \quad (5.8)$$

Hence, the two boundary conditions translate to the requirement of a well-convergent series of $\{a_{in}\}$ at both the starting region $[y_0 = 0, y_1]$ and the ending region $[y_{M-1}, y_M = 1]$. The basic idea of solving the eigenvalue problem is then clear. We use the strategy of try and test. Given the parity l , we make an initial guess for ν_m , and setup the series $\{a_{in}\}$ at the starting region $[y_0 = 0, y_1]$, and then propagate it to the ending region of $[y_{M-1}, y_M = 1]$. If the series converges at $y = 1$, then we find a correct eigenvalue and eigenfunction of the problem. Otherwise, we scan the value of ν_m , until all the required low-lying eigenvalues are found.

In greater detail, we apply the try and test strategy as follows. **(A)** At first, let us approximate, at each region $[y_i, y_{i+1}]$,

$$-(1-y)^2 \frac{dA}{dy} = \tilde{p}_0 + \tilde{p}_1 y + \tilde{p}_2 y^2, \quad (5.9)$$

$$-(1-y)^2 \tilde{A}_1(y) = \tilde{q}_0 + \tilde{q}_1 y + \tilde{q}_2 y^2. \quad (5.10)$$

To make the expansion accurate, generally we take $M \sim 30$. By introducing a new variable $z = y - y_i$, at the region $[y_i, y_{i+1}]$ we can cast the Eq. (5.6) into the form,

$$\left(\sum_{j=0}^3 r_j z^j \right) \frac{d^2 v}{dz^2} + \left(\sum_{j=0}^3 p_j z^j \right) \frac{dv}{dz} + \left(\sum_{j=0}^3 q_j z^j \right) v = 0, \quad (5.11)$$

where the coefficients $\{r_i\}$, $\{p_i\}$ and $\{q_i\}$ can be calculated directly from $\{\tilde{p}_i\}$ and $\{\tilde{q}_i\}$ in the program. We then substitute the solution $v(z) = \sum_{n=0}^{\infty} a_{in} z^n$ into the above equation to obtain the iterative relation (without confusion, here we denote $a_n \equiv a_{in}$ for this region),

$$\begin{aligned} a_{n+2} = & -\frac{(n+1)(nr_1 + p_0)}{(n+2)(n+1)r_0} a_{n+1} \\ & -\frac{[n(n-1)r_2 + np_1 + q_0]}{(n+2)(n+1)r_0} a_n \\ & -\frac{[(n-1)(n-2)r_3 + (n-1)p_2 + q_1]}{(n+2)(n+1)r_0} a_{n-1} \\ & -\frac{[(n-2)p_3 + q_2]}{(n+2)(n+1)r_0}. \end{aligned} \quad (5.12)$$

We need to classify two cases. (i) In the starting region of $y_0 = 0$, we have $r_0 = 0$ due to the boundary condition. Up to an overall irrelevant factor, we can set $a_0 = 1$ and then $a_1 = -q_0/p_0$. (ii) In the other regions, a_0 and a_1 are determined by the continuous conditions as stated below. Once a_0 and a_1 are known, we could obtain all the values of a_n by Eq. (5.12) since $a_{-1} = a_{-2} = 0$. Usually it is already sufficiently accurate to keep $n \leq n_{\max} = 16$. (B) The series $\{a_{in}\}$ at different regions are connected by the requirement that the function $v(y)$

and its first derivation $v'(y)$ should be continuous at the point $\{y_i\}$, where the index i runs from 1 to $M - 1$. (C) In this way, we can finally obtain the series $\{a_{in}\}$ at the region $[y_{M-1}, y_M]$. We judge the convergence by checking whether the value of $a_{M, n_{\max}}$ is sufficiently small or not.

In practise, the above procedure of solving the 1D hydrodynamic equation of a multi-component Fermi gas is very efficient and accurate. It can be applied as well to other 1D systems, such as the 1D interacting Bose gas, and to the 3D systems in spherical harmonic traps.

-
- [1] S. Inouye *et al.*, Nature (London) **392**, 151 (1998).
 - [2] M. Greiner *et al.*, Nature (London) **415**, 39 (2002).
 - [3] H. Hu, P. D. Drummond, and X.-J. Liu, Nature Physics **3**, 469 (2007), and references therein.
 - [4] A. J. Leggett, *Modern Trends in the Theory of Condensed Matter* (Springer-Verlag, Berlin, 1980).
 - [5] P. Nozières, and S. Schmitt-Rink, J. Low Temp. Phys. **59**, 195 (1985).
 - [6] J. R. Engelbrecht, M. Randeria, and C. A. R. Sá de Melo, Phys. Rev. B **55**, 15153 (1997).
 - [7] Y. Ohashi and A. Griffin, Phys. Rev. Lett. **89**, 130402 (2002).
 - [8] R. Haussmann *et al.*, Phys. Rev. A **75**, 023610 (2007).
 - [9] H. Hu *et al.*, Phys. Rev. Lett. **93**, 190403 (2004).
 - [10] H. Hu, X.-J. Liu, and P. D. Drummond, Europhys. Lett. **74**, 574 (2006).
 - [11] C. A. Regal and D. S. Jin, Phys. Rev. Lett. **92**, 040403 (2004).
 - [12] M. W. Zwierlein *et al.*, Phys. Rev. Lett. **92**, 120403 (2004).
 - [13] J. Kinast *et al.*, Phys. Rev. Lett. **92**, 150402 (2004).
 - [14] C. Chin *et al.*, Science **305**, 1128 (2004).
 - [15] T. Bourdel *et al.*, Phys. Rev. Lett. **93**, 050401 (2004).
 - [16] M. W. Zwierlein *et al.*, Nature (London) **435**, 1047 (2005).
 - [17] G. B. Partridge *et al.*, Phys. Rev. Lett. **95**, 020404 (2005).
 - [18] G. B. Partridge *et al.*, Science **311**, 503 (2006).
 - [19] T. Luu and A. Schwenk, Phys. Rev. Lett. **98**, 103202 (2007).
 - [20] V. Efimov, Nucl. Phys. A **210**, 157 (1973).
 - [21] T. Kraemer *et al.*, Nature **440**, 315 (2006).
 - [22] Ákos Rapp, G. Zaránd, C. Honerkamp, and W. Hofstetter, Phys. Rev. Lett. **98**, 160405 (2007).
 - [23] D. Bailin and A. Love, Phys. Rep. **107**, 325 (1984).
 - [24] M. G. Alford, K. Rajagopal, F. Wilczek, Phys. Lett. B **422**, 247 (1998); M. A. Halasz, A. D. Jackson, R. E. Shrock, M. A. Stephanov, and J. J. M. Verbaarschot, Phys. Rev. D **58**, 096007 (1998).
 - [25] C. R. Allton, S. Ejiri, S. J. Hands, O. Kaczmarek, F. Karsch, E. Laermann, Ch. Schmidt, and L. Scorzato, Phys. Rev. D **66**, 074507 (2002).
 - [26] H. Moritz, T. Stöferle, M. Köhl, and T. Esslinger, Phys. Rev. Lett. **91**, 250402 (2003).
 - [27] M. Bartenstein *et al.*, Phys. Rev. Lett. **94**, 103201 (2005).
 - [28] C. Honerkamp and W. Hofstetter, Phys. Rev. Lett. **92**, 170403 (2004).
 - [29] C. Honerkamp and W. Hofstetter, Phys. Rev. B **70**, 094521 (2004).
 - [30] T. Paananen, J.-P. Martikainen, and P. Törmä, Phys. Rev. A **73**, 053606 (2006).
 - [31] L. He, M. Jin, and P. Zhuang, Phys. Rev. A **74**, 033604 (2006).
 - [32] R. W. Cherng, G. Refael, and E. Demler, arXiv:cond-mat/0705.0347v1.
 - [33] P. F. Bedaque and J. P. D'Incao, arXiv:cond-mat/0602525.
 - [34] H. Zhai, Phys. Rev. A **75**, 031603(R) (2007).
 - [35] A. Sedrakian and J. W. Clark, Phys. Rev. C **73**, 035803 (2006).
 - [36] T. Paananen, P. Törmä, and J.-P. Martikainen, Phys. Rev. A **75**, 023622 (2007).
 - [37] E. H. Lieb and W. Liniger, Phys. Rev. **130**, 1605 (1963).
 - [38] C. N. Yang, Phys. Rev. Lett. **19**, 1312 (1967).
 - [39] M. Gaudin, Phys. Lett. **24A**, 55 (1967).
 - [40] T. Takahashi, *Thermodynamics of One-Dimensional Solvable Models* (Cambridge University Press, Cambridge, 1999).
 - [41] T. Bergeman, M. G. Moore, and M. Olshanii, Phys. Rev. Lett. **91**, 163201 (2003).
 - [42] G. E. Astrakharchik, D. Blume, S. Giorgini, and L. P. Pitaevskii, Phys. Rev. Lett. **93**, 050402 (2004).
 - [43] Note the difference in the definition of a_ρ with [41], which accounts for $A = -\zeta(1/2)/\sqrt{2} \simeq 1.0326$.
 - [44] I. B. McGuire, J. Math. Phys. **5**, 622 (1964); H. B. Thacker, Rev. Mod. Phys. **53**, 253 (1981).
 - [45] P. D. Drummond, R. M. Shelby, S. R. Friberg and Y. Yamamoto, Nature **365**, 307 (1993).
 - [46] K. S. Strecker, G. B. Partridge, A. G. Truscott, and R. G. Hulet, Nature **417**, 150 (2002); L. Khaykovich, F. Schreck, G. Ferrari, T. Bourdel, J. Cubizolles, L. D. Carr, Y. Castin, C. Salomon, Science **296**, 1290 (2002); Simon L. Cornish, Sarah T. Thompson, and Carl E. Wieman, Phys. Rev. Lett. **96**, 170401 (2006).
 - [47] W. Zwerger, J. Opt. B: Quantum Semiclass. Opt. **5**, S9 (2003).
 - [48] X.-J. Liu, P. D. Drummond, and H. Hu, Phys. Rev. Lett. **94**, 136406 (2005).
 - [49] H. Hu, X.-J. Liu, and P. D. Drummond, Phys. Rev. Lett. **98**, 070403 (2007).
 - [50] M. T. Batchelor *et al.*, Journal of Physics Conference Series **42**, 5 (2006).
 - [51] X.-W. Guan *et al.*, Phys. Rev. B **76**, 085120 (2007).
 - [52] X.-W. Guan *et al.*, To be published.
 - [53] M. Takahashi, Prog. Theor. Phys. **44**, 899 (1970).
 - [54] M. D. Girardeau, J. Math. Phys. **1**, 516 (1960).
 - [55] H. Heiselberg, Phys. Rev. A **63**, 043606 (2001).
 - [56] C. Menotti and S. Stringari, Phys. Rev. A **66**, 043610 (2002).

- [57] A. Minguzzi, P. Vignolo, M. L. Chiofalo, and M. P. Tosi, Phys. Rev. A **64**, 033605 (2001).